International Journal of Biological Macromolecules 259 (2024) 129143

Contents lists available at ScienceDirect

International Journal of Biological Macromolecules

journal homepage: www.elsevier.com/locate/ijbiomac

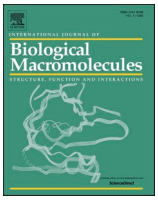

Interaction of food colorant indigo carmine with human and bovine serum albumins: A multispectroscopic, calorimetric, and theoretical investigation

Gouranga Jana, Shukdeb Sing, Arindam Das, Anirban Basu *

Department of Chemistry, Vidyasagar University, Midnapore 721 102, India

ARTICLE INFO

Keywords:
Food colorant
Indigo carmine
Serum albumin

ABSTRACT

In this work we have studied the interaction of the food dye Indigo-Carmine (IndC) with the most studied model transport proteins i.e. human and bovine serum albumin (HSA & BSA). A multispectroscopic approach was used to analyze the details of the binding process. The intrinsic fluorescence of both the albumins was significantly quenched by IndC and the quenching was both static and dynamic in nature with the former being dominant. The HSA-lndC and BSA-IndC distance after complexation was determined by Förster resonance energy transfer (FRET) method which suggested efficient energy transfer from the albumins to IndC. Thermodynamics of serum protein-IndC complexation was estimated by isothermal titration calorimetry (ITC) which revealed that the binding was enthalpy driven. Circular dichroism (CD) and FTIR spectroscopy revealed that the binding of IndC induced secondary structural changes in both the serum proteins. Synchronous and 3D fluorescence spectroscopy revealed that the binding interaction caused microenvironmental changes of protein fluorophores. Molecular docking analysis suggested that hydrogen bonding and hydrophobic interactions are the major forces involved in the complexation process.

1. Introduction

Indigo carmine (IndC, Fig. 1) is synthetic food dye produced by aromatic sulfonation of natural indigo. For its charming blue colour it is used in several food items such as jam, fruit juice, milk desserts and skim milk products [1]. It is also used as a diagnostic dye during surgical procedure (urological and gynecological surgery), in textile industry for dying clothes (blue, denim jeans), in cosmetics and capsule coating [2,3]. Though it has wide applications we can't ignore its potential toxicological effect on human body [4]. It causes skin and eye irritation on physical contact along with permanent damage of corona and conjunctiva of the eye [5]. Inhalation causes respiratory trouble due to irritation of respiratory tract. Intravenous administration to assess uretic potency can lead from mild to severe cardiovascular diseases and hypertension in patients [6–10]. Carcinogenic and tumor producing ability at application site has also been reported [10].

Serum albumin has become one of the most targeted macromolecular model proteins for drug-protein interaction studies due to its high abundance in blood plasma (40 mg ml^{-1}), target specific deposition and ability to transport a large number of exogenous and endogenous ligands. It also helps to maintain osmotic blood pressure and assists in adsorption and metabolism of drugs [11,12]. From the structural point of view BSA shows 75.80 % sequential resemblance with HSA. Three homologous domains I, II and III which can again be divided into two sub domains A & B form the heart shaped tertiary structure of serum proteins (both for HSA & BSA) [13–15]. Primary structure of HSA contains 585 and BSA consists of 583 amino acid residues [16]. Sub domain IIA (Sudlow site-I) and IIIA (Sudlow site-II) formed by hydrophobic cavity containing positively charged residues are the principal ligand binding sites [14,17]. A lot of research work on serum protein-small molecule interaction has been performed [18–20]. Due to the application of IndC in diverse fields there is a high possibility of mixing of IndC with body fluids. Therefore, it is highly pertinent to study the detailed binding mechanism and forces of interaction involved in IndC-serum albumin complexation. IndC-serum protein binding has not been explored yet apart from the works of Bonechi et al. through NMR relaxation [21]. Inevitably detail binding interaction study is essential for better understanding of the distribution, transportation and metabolism of the food colorant IndC in our body in order to realize its potential hazardous effects on human health. Therefore, the purpose of this work is to establish the detailed binding mechanism, thermodynamics, binding site and the forces involved in the complexation of IndC with

* Corresponding author.
E-mail address: anirbanbasu@mail.vidyasagar.ac.in (A. Basu).

https://doi.org/10.1016/j.ijbiomac.2023.129143
Received 6 November 2023; Received in revised form 21 December 2023; Accepted 28 December 2023
Available online 3 January 2024

serum albumins through multiple spectroscopic, calorimetric and molecular docking analyses for the very first time.

2. Experimental

2.1. Materials

Human serum albumin (≥99 % pure, CAS no. 70024–90-7) and citric acid (Lot# 120M0186V) were purchased from Sigma Aldrich chemical Co. (St. Louis, MO, USA). Bovine serum albumin (AR grade, CAS: 9048-46-5) and Indigo carmine (AR grade CAS: 860–22-0) were collected from Sisco Research Laboratories Pvt. Ltd. (SRL) India. Di-Sodium hydrogen phosphate was obtained from Merck (India) Limited. Double distilled water after filtration through 0.45 μm Millipore HA filter paper was used for citrate-phosphate (CP) buffer (pH 7.4, $[Na^+] = 10$ mM) preparation. A stock solution of HSA and BSA was prepared in CP buffer and its concentration was determined using the molar absorption coefficient values of 36,500 M^{-1} cm^{-1} and 43,800 M^{-1} cm^{-1} at 280 nm, respectively [22,23]. An aqueous stock solution of IndC was prepared and the concentration of IndC was 10^{-6} M for most of the experiments.

3. Methods

3.1. UV–visible spectral analysis

CP-buffer of pH 7.4 with 10 mM $[Na^+]$ concentration was used as the reference for all the UV–visible spectral measurements. Experiments were executed at 298.15 K in Shimadzu UV-1800 spectrophotometer, Japan. For the titration purpose 0–30 μM HSA was added to 15 μM IndC and 0–7 μM BSA was added to 20 μM IndC.

3.2. Steady-state fluorescence spectral analysis

Intrinsic fluorescence measurements were performed using quartz cuvette of 1 cm path length in Hitachi F-7000 spectrofluorimeter, Japan. The protein sample was excited at 295 nm and emission was recorded in the range of 305–450 nm maintaining temperature at 298.15 K. All the experiments were performed in CP buffer medium of pH 7.4 and $[Na^+] = 10$ mM. 4.96 μM HSA and 2.62 μM BSA were titrated with successive aliquots of IndC.

Synchronous fluorescence spectroscopy was performed keeping a fixed excitation-emission wavelength difference (Δλ) for tyrosine (Tyr) and Trp of 15 and 60 nm, respectively. The excitation and emission slit widths were kept 5 nm for all the synchronous fluorescence studies.

Red edge excitation shift (REES) was carried out by exciting the samples first at 295 nm and then at 305 nm for the native proteins as well as HSA-IndC and BSA-IndC complexes.

Excitation emission matrix analysis (3D fluorescence) was performed in the same instrument as mentioned above using 3D mode at a scan rate of 12,000 nm/min. Excitation and emission slit widths were 5 nm for all experiments. The concentration ratios i.e. [HSA]: [IndC] and [BSA]: [IndC] were 1:6 in both cases.

3.3. Time resolved fluorescence measurements

Horiba DeltaFlex™ modular fluorescence lifetime system (Glasgow, UK) was used for time resolved fluorescence measurements using time correlated single photon counting (TCSPC) method by exciting the samples at 288 nm using delta diode-C1 laser fixing the emission wavelength at 340 nm. Horiba EZ time analyzer software was used for the analysis purpose. The decay profile was given by the following exponential function

$$F(t) = \sum \alpha_i exp\left(-\frac{t}{\tau_i}\right) \quad (1)$$

where $F(t)$ indicates the fluorescence intensity at time t and for i^{th} decay time constant is τ_i and pre-exponential factor is α_i.

3.4. Förster resonance energy transfer (FRET)

For FRET measurements fluorescence emission data of HSA and BSA were obtained from Hitachi F-7000 spectrophotometer and absorbance data of IndC was obtained from UV-1800 UV-spectrophotometer. These spectra of 1:1 complexes of HSA and BSA with IndC were overlapped in the range of 305-475 nm for calculation of overlap integral. Spectral data was collected at 298.15 K in CP buffer medium of pH 7.4.

3.5. Isothermal titration calorimetry (ITC)

Nano ITC of TA instruments (Waters, New Castle, USA) was used for the calorimetric titration at 298.15 K. After degasification 20 μM of HSA & BSA was taken in the calorimeter cell and 10 μl aliquots of degassed IndC (1.28 mM) from 250 μl auto controlled rotating (250 rpm) syringe was added to it. Dilution studies were conducted by titration of IndC in blank buffer solution maintaining similar reaction conditions. Heat of dilution was then subtracted from the heat evolved during complexation and analyzed using Nano Analyze Software supplied by the manufacturer. The analysis of the plot of corrected heat vs mole ratio provided the enthalpy of reaction (ΔH^0) and equilibrium binding constant (K_a). ΔG^0 and $T\Delta S^0$ were evaluated using the following thermodynamic equations.

$$\Delta G^0 = -RT\ ln\ K_a = \Delta H^0 - T\Delta S^0 \quad (2)$$

where T is the temperature in kelvin and R is the universal gas constant.

3.6. FTIR analysis

FTIR spectra of HSA and BSA and their complex with IndC was taken using Perkin-Elmer FTIR spectrophotometer (Spectrum two) version10.03.07 (Perkin-Elmer, Inc., USA) equipped with Lithium tantalate ($LiTaO_3$) MIR detector, KBr beam splitter in ZnSe attenuated

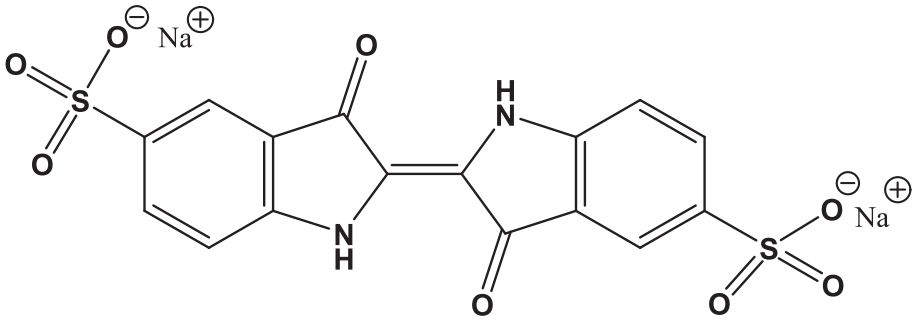

Fig. 1. Molecular structure of IndC.

total reflection (ATR) mode. For both HSA & BSA 1:5 protein- IndC ratio was maintained. All the spectra were recorded after back ground correction in CP buffer of pH 7.4.

3.7. Circular dichroism spectroscopy (CD)

For exploration of ligand induced conformational changes CD spectra of the serum albumins was studied using Jasco J-1100 CD Spectrometer (Hachioji, Tokyo, Japan) in 1 mm quartz cuvettes fixing the band with at 1 nm and scan rate at 100 nm/min. Peltier temperature controller (PTC-514) was used to control the temperature of the cell holder during experiments. Five successive scans were performed to minimize the signal to noise ratio.

3.8. Molecular docking analysis

Molecular docking is the software based theoretical study extensively used for studying protein-ligand binding interaction to find out the probable binding site and various binding parameters [24]. Crystal structure of HSA and BSA were taken from Protein Data Bank (https://www.rcsb.org) with pdb id 1AO6 [14] and 4F5S [13]. Structure of IndC was collected from Pubchem (https://pubchem.ncbi.nlm.nih.gov) with CID 2723854. At pre-docking stage proteins were prepared by subtracting water molecules and co-crystal ligands (if any) followed by addition of hydrogen by PROPKA 3.1 at pH 7.4 and appropriate Kollman charges [25] using AutoDockTools software (https://autodock.scripps.edu). Ground state electronics of IndC geometry were calculated using the Quantum Espresso (QE) code [26], which is a plane wave based execution of DFT (Density Functional Theory) [27]. BFGS scheme has been used to obtain the relaxed structures within the pseudo-potential used. The KS ground states are calculated within the Perdew-Burke-Ernzerhof (PBE) [28] approximation of the exchange-correlation functional. Plane wave basis with kinetic energy cutoff of 60 Rydberg has been used for all systems considered in this work. Then Gasteiger charges was also applied to IndC [29]. Protein-ligand docking was performed by AutoDock 4.2.6 (The Scripps Research Institute, TSRI). Docking was done taking grid box dimension 50 × 70 × 60 & 52 × 78 × 52 with center of grid point at (32.801, 37.931, 31.620) & (1.910, 29.303, 102.871) for HSA & BSA, respectively. For docking, Lamarckian Genetic algorithm [30] was applied over 50 runs with 2,500,000 energy evaluation. Docking results were analyzed by AutoDockTools and visualization of protein-ligand complex was done by BIOVIA Discovery studio.

3.9. Statistical analysis

The data reported are mean ± standard deviation (S.D.) of four independent determinations. The combined standard uncertainty $u_c(x)$ is given by.

$$u_c(x) = \left\{ (u_1(x))^2 + (u_2(x))^2 + (u_3(x))^2 + \ldots\ldots\ldots\ldots + \text{etc.} \right\}^{1/2} \quad (3)$$

where $u_1(x)$, $u_2(x)$, $u_3(x)$, etc. are the individual uncertainties in the data measurements.

4. Result and discussion

4.1. UV–visible spectral analysis

IndC gives strong absorption peaks at 609, 286 and 249 nm (Fig. S1). For our interaction study we have monitored the peak at 609 nm as it is not in the protein absorption region (Fig. 2).

There was gradual quenching of absorption spectra of IndC up to saturation without any significant alteration in peak position upon successive addition of both HSA and BSA.

4.2. Effect of IndC on intrinsic fluorescence spectra of HSA and BSA

For ascertaining the interaction and binding mechanism of protein and IndC steady state fluorescence quenching experiments were performed [31–33]. For HSA Trp214 (subdomain IIA), Tyr263 (subdomain IIA) and phenylalanine are mostly responsible for its intrinsic fluorescence. The contribution of Tyr263 and phenylalanine towards intrinsic fluorescence is negligible when excited at 295 nm. So, Trp214 plays the most important role towards its intrinsic fluorescence [34,35]. On the other hand, Trp213 and Trp134 are the two effective intrinsic fluorophores of BSA located at the hydrophobic pocket domain-II and surface of domain-I, respectively [36]. IndC progressively quenched the intrinsic fluorescence of HSA and BSA (Fig. 3) along with a 6 nm blue shift for HSA.

Three major factors inner filter effect, static quenching i.e. ground state complex formation and dynamic quenching are mainly responsible for intrinsic fluorescence quenching of serum albumins [31]. Inner filter effect correction was performed using the equation reported in literature [31]. After correction for IndC fluorescence and inner filter effect fluorescence data was analyzed using the following Stern-Volmer Eq. (4)

$$\frac{F_o}{F_{cor}} = 1 + K_q \tau_o [Q] = 1 + K_{SV}[Q] \quad (4)$$

where F_0 and F_{cor} signify the intrinsic fluorescence of serum albumin in

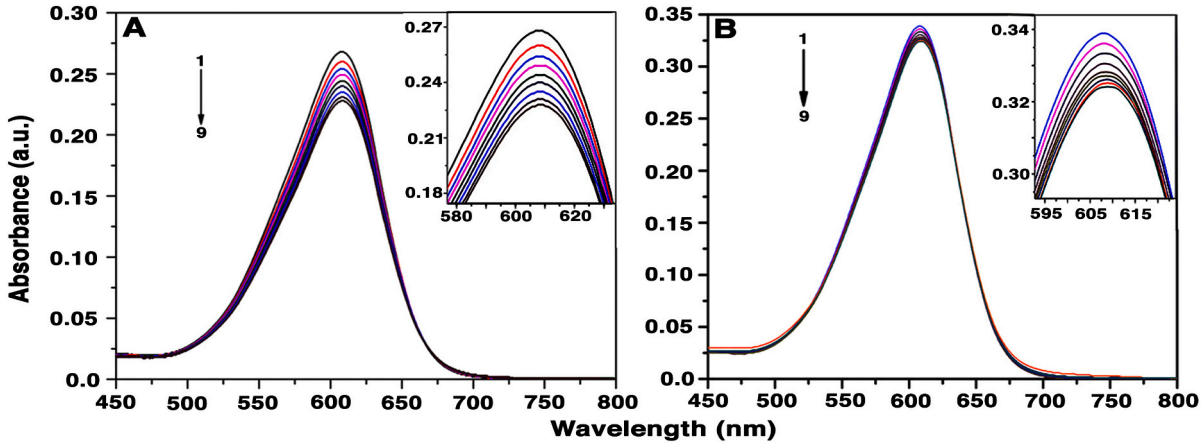

Fig. 2. Absorption spectral change of IndC upon treatment with (A) 0, 2.70, 5.40, 8.10, 11.70, 15.30, 19.80, 24.30, 29.70 (curves 1–9) μM HSA and (B) 0, 0.87, 1.75, 2.62, 3.50, 4.37, 5.24, 6.12, 6.99 μM (curves 1–9) BSA.

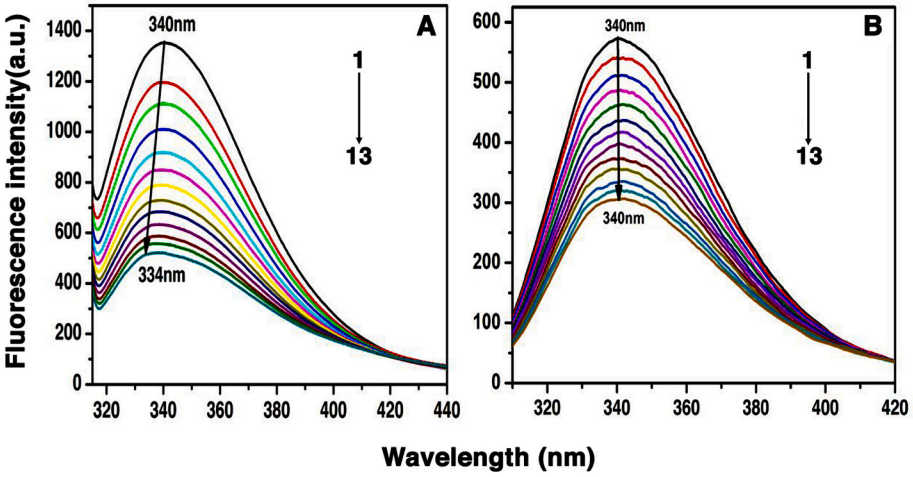

Fig. 3. Changes in the steady-state fluorescence spectra of (A) HSA (4.96 μM, curve 1) and (B) BSA (2.62 μM, curve 1) upon treatment with 1.28, 2.56, 3.84, 5.12, 6.40, 7.68, 8.96, 10.24, 11.52, 12.80, 14.08, 15.36 μM IndC (2 → 13 → 13).

absence and presence of IndC. K_q = quenching rate constant, [Q] = concentration of IndC, K_{SV} = Stern-Volmer quenching constant and τ_0, average life time of unquenched serum albumins, is in the order of 10^{-8} s [31]. The calculated K_{SV} values are $(1.35 \pm 0.06) \times 10^5$ M^{-1} for HSA and $(4.09 \pm 0.08) \times 10^4$ M^{-1} for BSA. Furthermore the value of K_q (K_{SV}/τ_0) was found to be $(1.35 \pm 0.06) \times 10^{13}$ M^{-1} s^{-1} and $(4.09 \pm 0.08) \times 10^{12}$ M^{-1} s^{-1}, respectively, for HSA and BSA which is much higher than the maximum limit of K_q for a diffusion controlled process involving a biopolymer [36–38]. Thus, static quenching mechanism played a significant role in overall quenching process. There exists another conflict about the contribution of dynamic quenching towards the overall quenching process. So, time resolved fluorescence study was performed for further elucidation of the quenching mechanism.

4.3. Time resolved fluorescence measurements

In many instances fluorophores can be quenched by a combined mechanism i.e. through both static and dynamic quenching. To separate out these two binding mechanisms time resolved fluorescence measurement is one of most authentic techniques [39]. We monitored the fluorescence decay of Trp residue which is an intrinsic fluorophore of both BSA and HSA at different concentrations of IndC. The decay profiles of HSA and BSA could be fitted to multiexponential function. We observed that the best fit was bi-exponential function for both BSA and HSA and also their complex with IndC (Fig. 4). The life time values (τ_1, τ_2) and their relative amplitudes (α_1, α_2) along with the calculated average lifetime <τ>, and suitable χ^2 values are tabulated in Table 1.

Using the equation $<\tau> = \Sigma\alpha_i\tau_i$ our calculated life time value for BSA and HSA were 5.86 and 5.72 ns, respectively, in agreement with the earlier reports [40]. From Table 1 the life time values show overall decreasing trend with increase in concentration of IndC which suggest dynamic quenching is also involved in the overall quenching process. For the evaluation of dynamic quenching constant, we use the equation [41].

$$\frac{\langle\tau_0\rangle}{\langle\tau\rangle} = 1 + K_D[Q] \quad (5)$$

where $<\tau_0>$ and $<\tau>$ indicate the average life time of serum protein (BSA and HSA) in the absence and presence of IndC, respectively. For the determination of dynamic quenching constant (K_D) Eq. (5) was used and from the slope of this linear plot (Fig. 5 A & B) K_D value was found to be $(1.40 \pm 0.03) \times 10^4$ and $(2.09 \pm 0.04) \times 10^4$ M^{-1}, respectively, for the

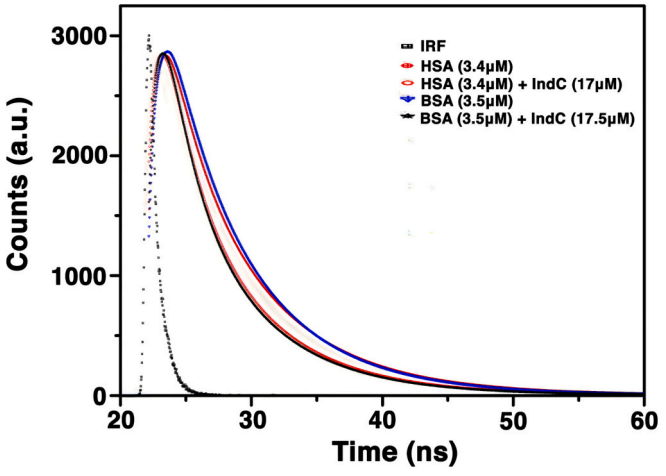

Fig. 4. Representative fluorescence life time decay profiles of HSA, BSA, HSA-IndC &BSA-IndC system.

Table 1
Effect of variation of concentrations of IndC on fluorescence life time of serum proteins.

Conc.(μM)	α_1	τ_1(ns)	α_2	τ_2(ns)	<τ>(ns)	χ2
HSA + IndC						
HSA(3.4 μM)	0.25	2.24	0.75	6.89	5.72	1.14
HSA(3.4 μM) + IndC(3.4 μM)	0.28	1.93	0.72	6.72	5.37	1.17
HSA(3.4 μM) + IndC(6.8 μM)	0.30	2.12	0.70	6.66	5.29	1.09
HSA(3.4 μM) + IndC(10.2 μM)	0.36	2.08	0.64	6.63	4.99	1.18
HSA(3.4 μM) + IndC(13.6 μM)	0.38	1.85	0.62	6.50	4.73	1.17
HSA(3.4 μM) + IndC(17 μM)	0.40	2.22	0.60	6.33	4.68	1.14
BSA + IndC						
BSA(3.5 μM)	0.28	3.44	0.72	6.80	5.86	1.09
BSA(3.5 μM) + IndC(3.5 μM)	0.27	2.37	0.73	6.51	5.39	1.15
BSA(3.5 μM) + IndC(7 μM)	0.32	2.13	0.68	6.37	5.01	1.11
BSA(3.5 μM) + IndC(10.5 μM)	0.37	2.18	0.67	6.37	4.81	1.22
BSA(3.5 μM) + IndC(14 μM)	0.42	2.00	0.58	6.27	4.47	1.16
BSA(3.5 μM) + IndC(17.5 μM)	0.44	1.92	0.56	6.15	4.28	1.17

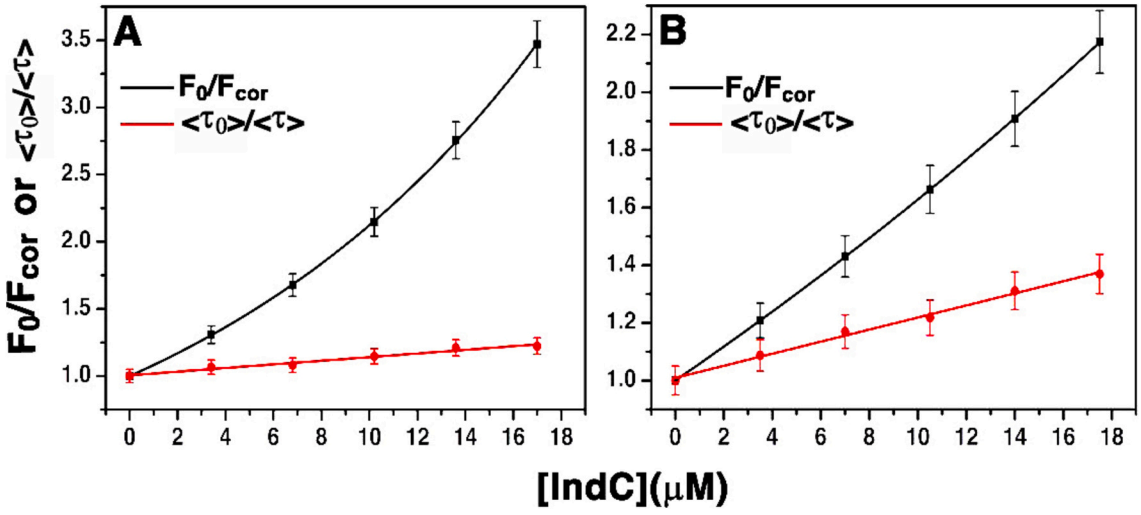

Fig. 5. Plot of F_0/F vs [IndC] (black line) and τ_0/τ vs [IndC] (red line) for (A) HSA-IndC system and (B) BSA-IndC system.

complexation of HSA and BSA with IndC. For calculation of static quenching constant (K_S) the following equation was used [41].

$$K_{app} = \left(\frac{F_o}{F_{cor}} - 1\right)\frac{1}{[Q]} = (K_s + K_D) + K_s K_D[Q] \tag{6}$$

From the plot of K_{app} versus [IndC] and using the value of dynamic quenching constant (K_D), the static quenching constant was determined to be (6.07 ± 0.09) × 10^4 M^{-1} and (3.67 ± 0.07) × 10^4 M^{-1}, respectively, for complexation of HSA and BSA with IndC. This data clearly shows that overall quenching process was a combination of both static and dynamic quenching mechanism but static quenching was dominant in the overall quenching process as the value of static quenching constant is higher than that of dynamic quenching constant [42–44].

4.4. Estimation of binding parameters

For independent binding of IndC to a specific binding site of HSA and BSA there must exist equilibrium between IndC bound protein and unbound protein. The binding constant was determined from the following modified double log equation [45,46].

$$log\frac{F_0 - F_{cor}}{F_{cor}} = nlogK_b - nlog\left[\frac{1}{\left\{[Q] - \frac{P_t(F_0 - F_{cor})}{F_0}\right\}}\right] \tag{7}$$

where P_t indicates protein concentration, K_b represents binding constant and n represents number of available binding sites per HSA/BSA. From the intercept of log [(F_0-F_{cor})/F_{cor}] vs log [1/{[Q]-P_t(F_0-F_{cor})/F_{cor}}] plot (Fig. S2) the binding constant for HSA and BSA was calculated to be (3.63 ± 0.20) × 10^4 and (5.30±±0.60) × 10^4 M^{-1}, respectively, in 10 mM CP buffer. The number of binding sites (n) calculated from the slope of plot was (0.87 ± 0.01) for HSA and (1.03 ± 0.03) for BSA. Evidently there was only one type of binding site for IndC on the serum proteins.

4.5. Förster resonance energy transfer (FRET)

Excited state energy transfer can be evidence for complex formation between the serum protein and IndC. The proximity of protein binding site with the ligand molecule can be effectively calculated from the energy transfer efficacy. To understand the structural and

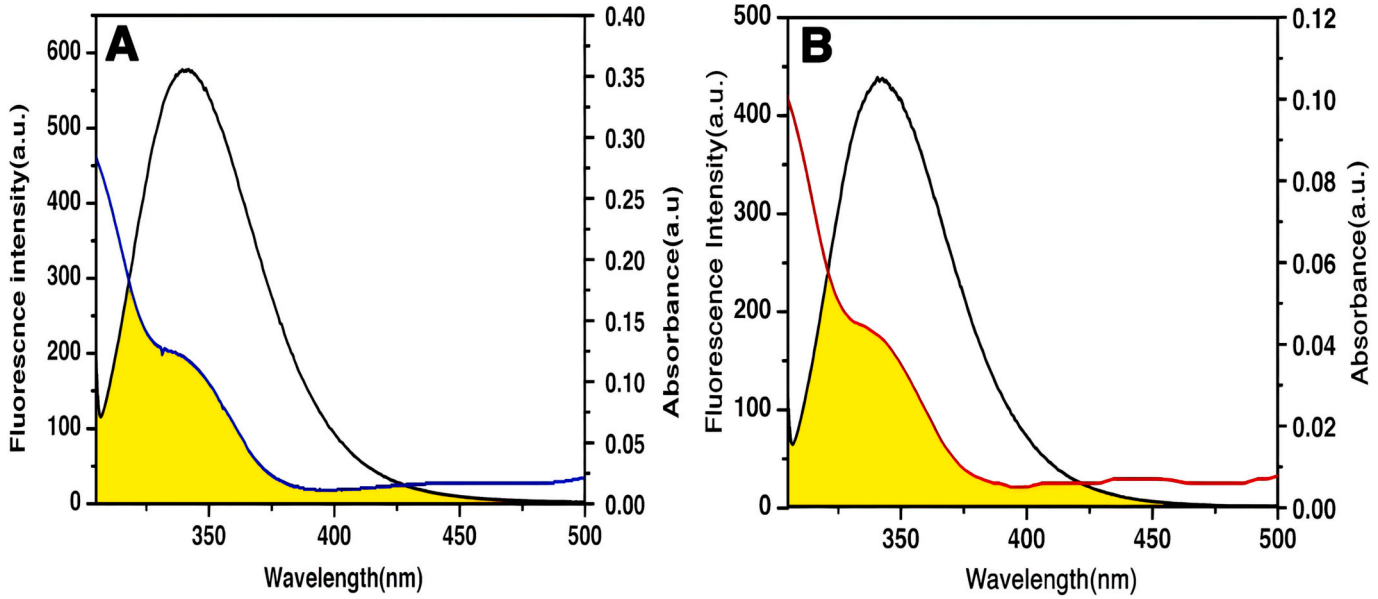

Fig. 6. Overlap (yellow portion) between the emission spectrum of (A) HSA & (B) BSA and absorption spectrum of IndC. In both cases protein-IndC ratio remain 1:1.

conformational alteration associated with binding process this knowledge is critical [47]. It is considered that donor-accepter partner remains within Förster distance when there exists an overlap between the emission spectrum of serum protein and absorption spectrum of IndC (Fig. 6).

Energy transfer efficiency (E), according to non radiative energy transfer theory of Förster [48] is given by the following equation

$$E = 1 - \frac{F}{F_0} = \frac{R_0^6}{R_0^6 + r^6} \tag{8}$$

where F and F_0 are the intrinsic fluorescence intensities of serum proteins in presence and absence of IndC. r is the distance between serum protein and IndC. Förster radius (R_0) indicates the critical distance between the binding site of serum protein and IndC when 50 % excited energy transfer has been completed [48]. It was calculated using the following relation

$$R_o^{\ 6} = 8.8 \times 10^{-25} k^2 n^{-4} \varphi J \tag{9}$$

where k^2 signify the absorption and emission dipolar special orientation factor, n indicates refractive index of the medium, ϕ indicates fluorescence quantum yield of serum protein. J designates the overlap integral of emission spectrum of serum protein and absorption spectrum of IndC. J is given by the following equation

$$J = \frac{\int_0^\infty F(\lambda)\varepsilon(\lambda)\lambda^4 d\lambda}{\int_0^\infty F(\lambda) d\lambda} \tag{10}$$

where $F(\lambda)$ is fluorescence intensity of serum protein at wavelength λ, $\varepsilon(\lambda)$ is the molar absorption coefficient of IndC at wavelength λ. For serum protein considering the value of $k^2 = 2/3$, $n = 1.336$, and φ =0.15 [49,50] and using the above equation the value of E, J, R_0, and r were evaluated to be 0.345, 1.32×10^{-14} cm^3 L mol^{-1}, 2.47 and 2.746 nms for HSA and 0.165, 6.42×10^{-15} cm^3 L mol^{-1}, 2.45 and 3.21 nms for BSA. Evidently the distance between the binding Trp residue of the serum protein and IndC was much lower than 8 nm (the maximum limiting distance between donor and accepter for efficient energy transfer process) indicating that efficient energy transfer takes place from the serum proteins to IndC. The higher value of r compared to R_0 and efficient energy transfer provide evidence for the ground-state complex formation between the two interacting species [51].

4.6. FTIR analysis

FTIR is a technique by which secondary structural changes in HSA/BSA upon binding with small molecules can be qualitatively studied specially in the amide region of the protein molecule. Two main analyzing domains of HSA/BSA are amide-I due to C═O stretching frequency and amide-II which arises due to coupled N—H bending and C—N stretching [52,53]. Spectral alliance clearly shows that amide region is mostly affected upon binding with IndC. Spectral shift of 1653 to 1655 cm^{-1} for HSA and 1653 to 1651 cm^{-1} for BSA is observed in amide-I region upon complexation (Fig. 7A & B). In case of HSA the amide-II region peak at 1549 cm^{-1} remain unaltered but additionally peaks appeared at 1530 and 1567 cm^{-1} after treatment with IndC (Fig. 7A & B). For BSA the peak was observed at 1546 cm^{-1} (C—N stretching coupled with N—H bending) but in the BSA-IndC adduct the peaks were observed at 1544 and 1556 cm^{-1} [53,54]. Decrease in intensity of amide-I band at 1653 cm^{-1} of native HSA/BSA after complex formation indicated that percentage of α-helix of the serum albumins was decreased in presence of IndC [55,56].

4.7. Synchronous fluorescence studies

Conformational alteration of serum protein due to binding with IndC can be evaluated through synchronous fluorescence analysis. Synchronous fluorescence spectra apprize us of microenvironmental changes around the protein residues. Difference in excitation and emission wavelength (Δλ), when fixed at 15 nm lend information about Tyr residues whereas at Δλ = 60 nm it lends information about the Trp residues [57]. Effect of IndC on the synchronous fluorescence spectra (excitation) of HSA and BSA are shown in Fig. 8. Synchronous fluorescence spectra was significantly quenched for both BSA and HSA in presence of IndC but only 2 nm (277 to 275 nm, Fig. 8A) blue shift was observed in case of HSA when Δλ was fixed at 60 nm. This observation suggests Trp residue enter into more hydrophobic region associated with a conformational change in HSA. For BSA such shift in the emission maxima was not observed for both Δλ = 15 & 60 nm indicating that the microenvironmental polarity around the protein fluorophores remained almost same upon binding with IndC [58].

4.8. Recognition of complex formation through ITC

Bimolecular interactions can be effectively studied through ITC [59]. ITC thermograms for the complexation of HSA and BSA with IndC at 298.15 K is depicted in Fig. 9A & B. Exothermic reactions were observed in both cases. The corrected heat was obtained after subtraction of heat of dilution of IndC which was determined from a blank titration using only buffer and identical amount of IndC. Lower panel of the thermograms (Fig. 9A & B) represent the plot of corrected heat vs mole ratio of

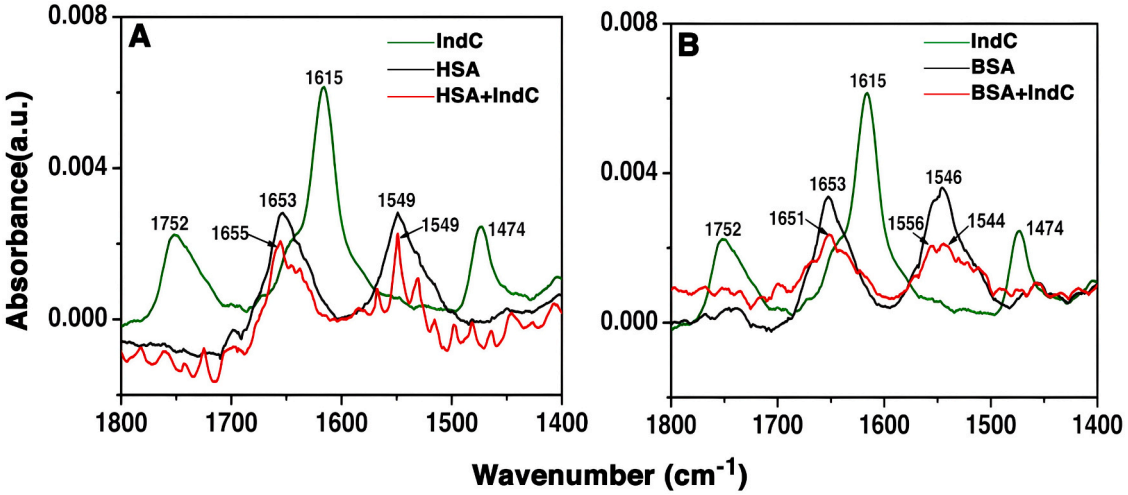

Fig. 7. FTIR spectra of IndC, (A) HSA and its complex with IndC & (B) BSA and its complex with IndC.

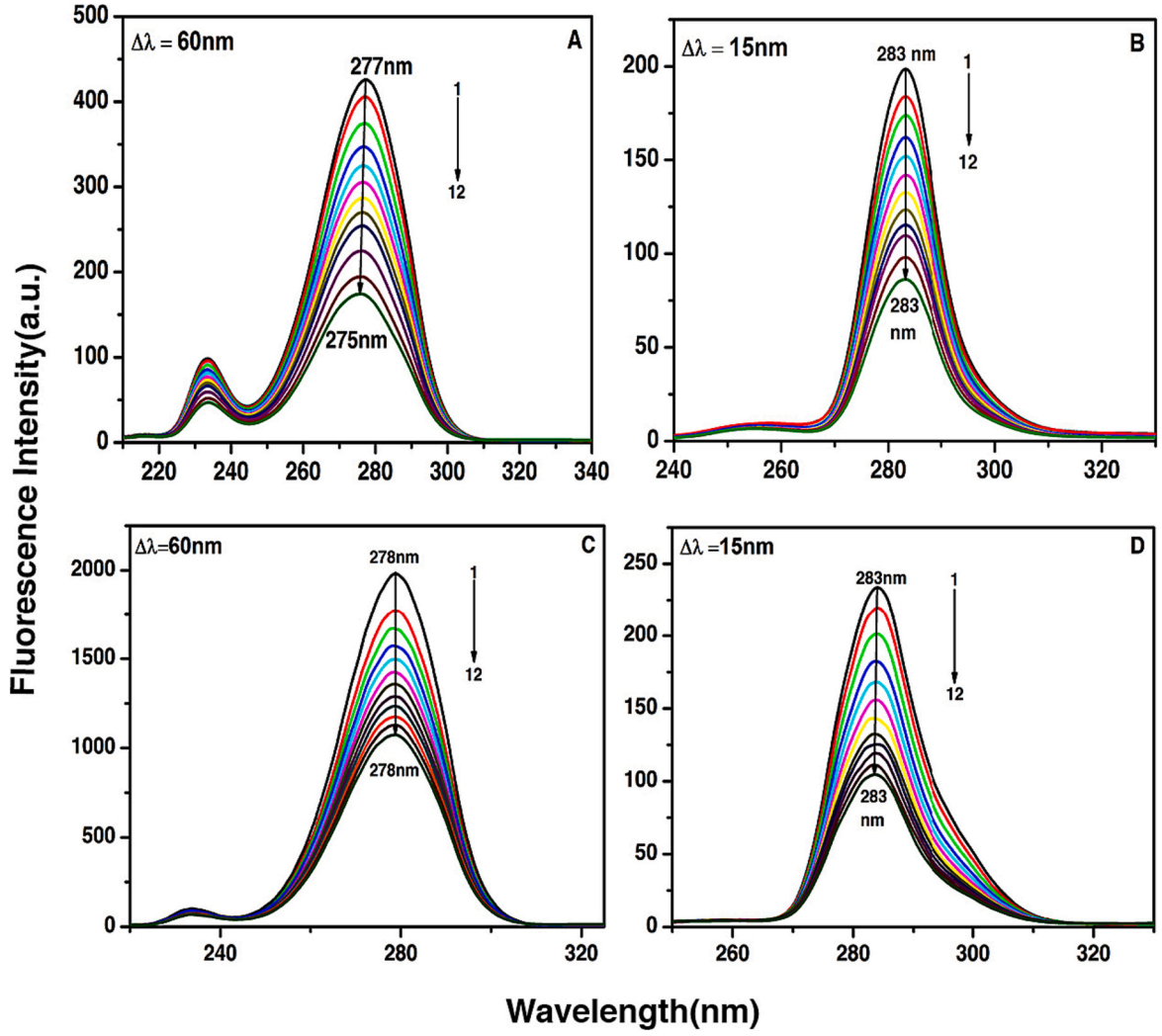

Fig. 8. Synchronous fluorescence (excitation) spectra of HSA (curve 1 of panels A & B) and BSA (curve 1 of panels C & D) in the presence of 1.28, 2.56, 3.84, 5.12, 6.40, 7.68, 8.96, 10.24, 11.52,12.80, 14.08 μM IndC (curves 2–12).

IndC. Binding constants (K_a) obtained from ITC for the complexation of HSA and BSA with IndC were (4.06 ± 0.30) × 10^4 and (9.39 ± 0.50) × 10^4 M^{-1}, respectively. A large negative standard molar enthalpic component was the main driving force for the complexation of serum proteins with IndC (Table 2). The high negative ΔH^0 value is the outcome of the tightening of hydrogen bonding interactions at macromolecular interior where low dielectric medium is present along with the hydrophobic interactions [60,61]. The negative ΔG^0 values of -(6.29 ± 0.30) and –(6.78 ± 0.50) kcal/mol for HSA and BSA, respectively, suggested spontaneous complex formation takes place between the serum proteins and IndC.

4.9. Ligand induced conformational changes

For monitoring the IndC induced secondary structural changes in serum proteins circular dichroism (CD) study was performed keeping a fixed concentration of serum protein and varying the concentrations of IndC. Information about the percentage change of α-helix, β-sheet and random coil of HSA/BSA upon binding with IndC can be generated from CD studies [62]. Spectral changes in HSA and BSA upon addition of IndC is shown in Fig. 10. Two negative peaks in HSA and BSA at 208 and 222 nm comes from π → π* transition of α-helix and n → π* transition of α-helix along with the random coil [63]. The magnitude of spectral reduction upon increasing the concentration of IndC signify the extent of secondary structural changes in HSA/BSA moiety during binding. For calculation of percentage of helical content following equations were used [64].

$$\mathrm{MRE}[\theta]_{\lambda} = \frac{\text{observed CD}(\mathrm{m}\,deg)}{\mathrm{Cnl} \times 10} \tag{11}$$

Here MRE indicates the mean residual ellipticity (deg.cm^2.$dmol^{-1}$) and C, n and l are concentration (M) of serum protein, total number of residues and cuvette path length (cm), respectively. The percentage of α-helix of HSA/BSA was evaluated using following equation

$$\alpha - helix(\%) = \left[\frac{[\theta]_{208} - 4000}{33000 - 4000}\right] \times 100 \tag{12}$$

The percentage of α-helix decreased from 66.09 to 45.75 % for HSA and from 52.46 to 31.51 % for BSA after treatment with IndC. Though the α-helical content decreased during interaction but still it is predominant after interaction. No significant change was observed in the near UV CD spectrum (Fig. S4) of the serum proteins in the wavelength range 250–320 nm.

4.10. Red edge excitation shift (REES)

REES implies the shift in the fluorescence emission maxima towards longer wavelength when excitation is shifted towards the red edge of the

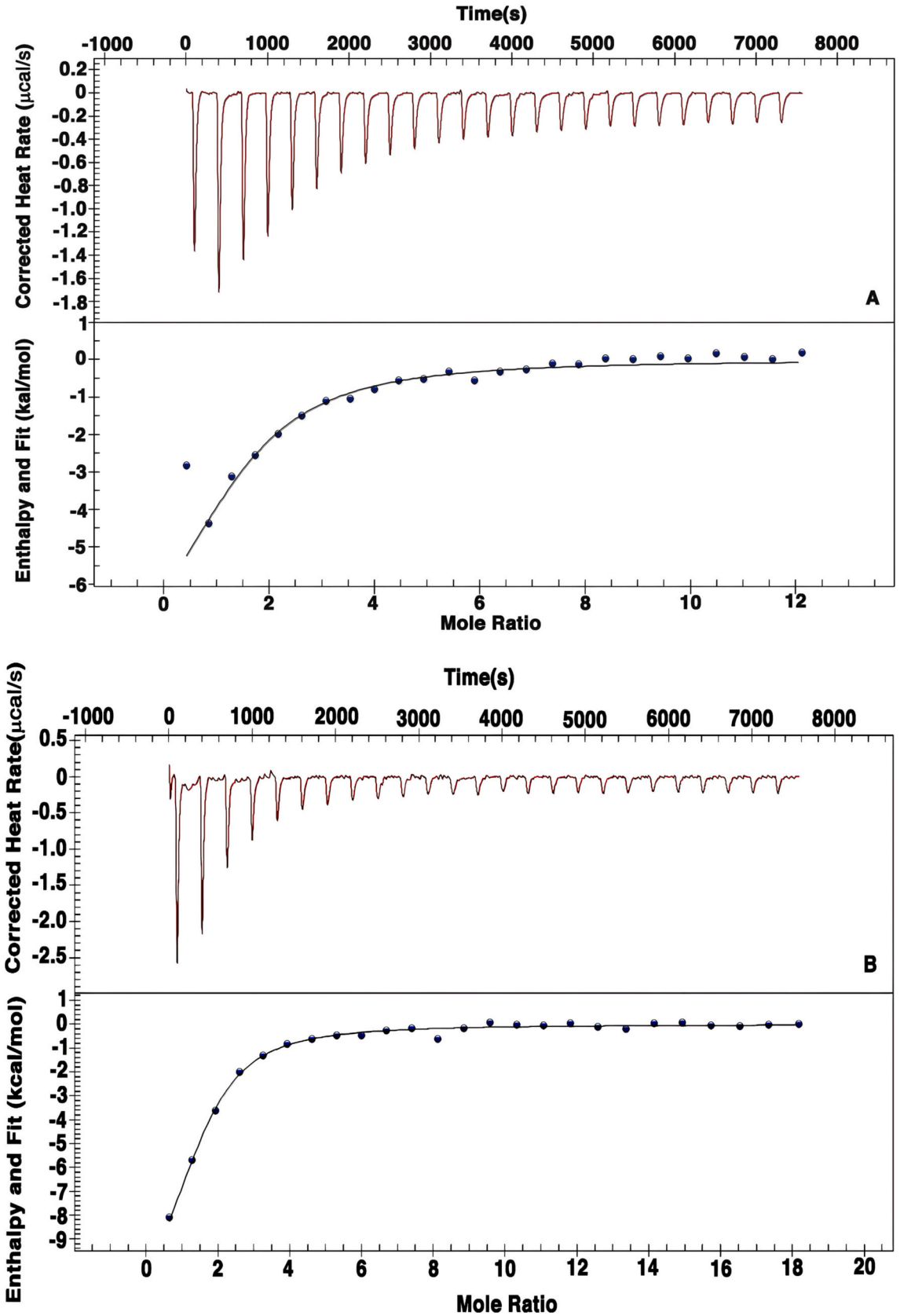

Fig. 9. Isothermal titration calorimetric profile for the complexation of IndC with (A) HSA and (B) BSA at 298.15 K. The upper panel of thermogram shows the sequential injection of IndC (1.28 mM) into the solutions of HSA (20 μM) and BSA (20 μM) and lower panel is the plot of corrected heat in integrated form vs mole ratio. The data were fitted to one binding site model and the best fit of the data is indicated by the solid line in the lower panel.

Table 2
Thermodynamic parameters evaluated from ITC experiment at 298.15 K.

System	K_a (M^{-1}) × 10^{-4}	ΔH^o (kcal/mol)	$T\Delta S^o$ (kcal/mol)	ΔG^o(kcal/mol)	n
HSA	4.06 ± 0.30	−9.24 ± 0.20	−2.95 ± 0.10	−6.29 ± 0.30	1.32 ± 0.02
BSA	9.39 ± 0.50	−13.30 ± 0.40	−6.52 ± 0.10	−6.78 ± 0.50	1.27 ± 0.05

spectrum. It can be effectively used to examine the environmental rigidity and dynamics in the proximity of protein fluorophores [65]. For observation of REES effect, we excite the Trp residue of native protein (HSA and BSA), HSA-IndC and BSA-IndC complex first at 295 nm and then at 305 nm. Results are depicted in Table 3 where $\Delta\lambda_{em,max}$ indicates the difference in emission maxima when the protein fluorophores were excited at two different wavelengths. Native HSA shows 3 nm REES effect whereas after complexation with IndC it rises to 10 nm. This result indicates that motional restriction around the Trp residue increased to a great extent upon complexation. BSA does not show any significant shift but after complex formation with IndC 4 nm REES effect was observed. Therefore, more restriction was imposed on the microenvironment of the Trp residues upon complexation with IndC [45,66].

4.11. Excitation emission matrix analysis or 3D fluorescence analysis

In recent times 3D fluorescence spectra has received special attention as it generates information about the microenvironmental and conformational changes in the immediate vicinity of the protein fluorophores upon binding to a ligand. The effect of IndC on the 3D fluorescence spectra of the serum albumins is presented in Fig. 11 and the related information in table S1. As depicted in the figure peak-a corresponds to the first order Rayleigh scattering at $\lambda_{ex} = \lambda_{em}$ whereas other two peaks i.e. peak-1 indicates spectral characteristics of Trp and Tyr residues and peak-2 arises due to the polypeptide backbone of serum albumins [45,67]. In both the cases (HSA & BSA) fluorescence intensity diminished to a large extent. For HSA stokes shift ($\Delta\lambda$) decreased by 5 and 2 nm, respectively, for peak-1 and peak-2. This result indicated the conformational changes around the Trp residues and polypeptide backbone upon binding with IndC. For BSA-IndC complex 2 nm stokes shift ($\Delta\lambda$) was observed for peak-1 but no alteration in stokes shift ($\Delta\lambda$) was observed for peak-2. This result signifies that though BSA is homologous to HSA but the binding process is slightly different as it changes the microenvironment surrounding the Trp residues without affecting the polypeptide backbone.

4.12. Molecular docking analysis

In silico investigations were performed to explore the probable binding site of IndC in HSA and BSA maintaining RMSD tolerance 2Å **.** In IndC molecule there are 6 active torsions between S-1 and O-5, S-1 and O-23, S-2 and O-6, S-2 and C-26, O-3 and C-17, C-13 and C-16. Heterocyclic molecules with negative charge generally bind at Sudlow site-I and negatively charged molecules containing carboxylic acid choose sudlow site-II for their binding [17]. Best docking conformer has lowest binding energy of −6.41 and − 7.29 kcal/mol, respectively, for HSA and BSA (table S2). Best docking conformer of IndC preferably bind at sudlow site-I (subdomain-IIA of hydrophobic pocket) of both HSA and BSA (Fig. 12A & C**).** Moreover, docking study clearly provides information about the intrinsic fluorophores of HSA i.e. Trp-214 which actively participates in binding through π-sulphur and π-π T-shaped interaction. For BSA the intrinsic fluorophore Trp-213 is involved in binding through van der Waals interaction (Fig. 12 B & D). Hydrogen bonding contributes significantly to the total binding energy as IndC forms three conventional hydrogen bonds with HSA. The terminal sulphate groups and carbonyl group of IndC participates in hydrogen bonding with ARG A:222 (2.84 Å, 2.42 Å) and SER A:287 (2.25 Å) of HSA (Fig. S4). IndC forms six conventional hydrogen bonds with TYR A:149 (2.93 Å), ARG A:256 (2.57 Å), HIS A:241 (1.89 Å), THR A:190 (3.06 Å), TYR A:156 (2.47 Å) and TYR A:451 (2.18 Å) of BSA (Fig. S5). Hydrophobic interaction is another contributing factor towards the total binding energy. TRP A:214, ALA A:291, HIS A:242, LYS A:195, ARG A:222 and SER A:287 are the residues involved in hydrophobic

Table 3
Shift in emission maxima ($\Delta\lambda$) upon change in excitation wavelength (λ_{ex}).

System	$\lambda_{em,max}$(nm)		$\Delta\lambda_{em,max}$(nm)
	λ_{ex} = 295 nm	λ_{ex} = 305 nm	
HSA	339	342	3
HSA + IndC	333	343	10
BSA	342	342	0
BSA + IndC	340	344	4

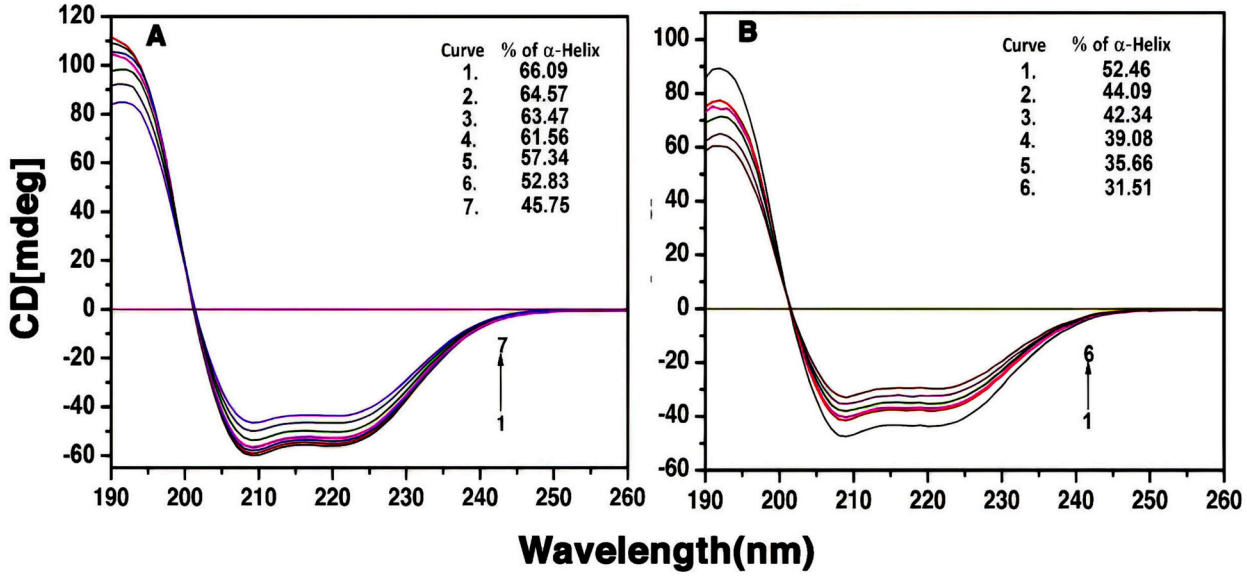

Fig. 10. Far UV CD spectral changes in (A) HSA (curve1, 4.5 μM) on treatment with 2, 4, 7, 10, 20, 30 μM (curves 2 → 7) IndC and (B) BSA (curve1, 4.2 μM) on treatment with 1, 4, 7, 20, 30 μM (curves 2 → 6) IndC.

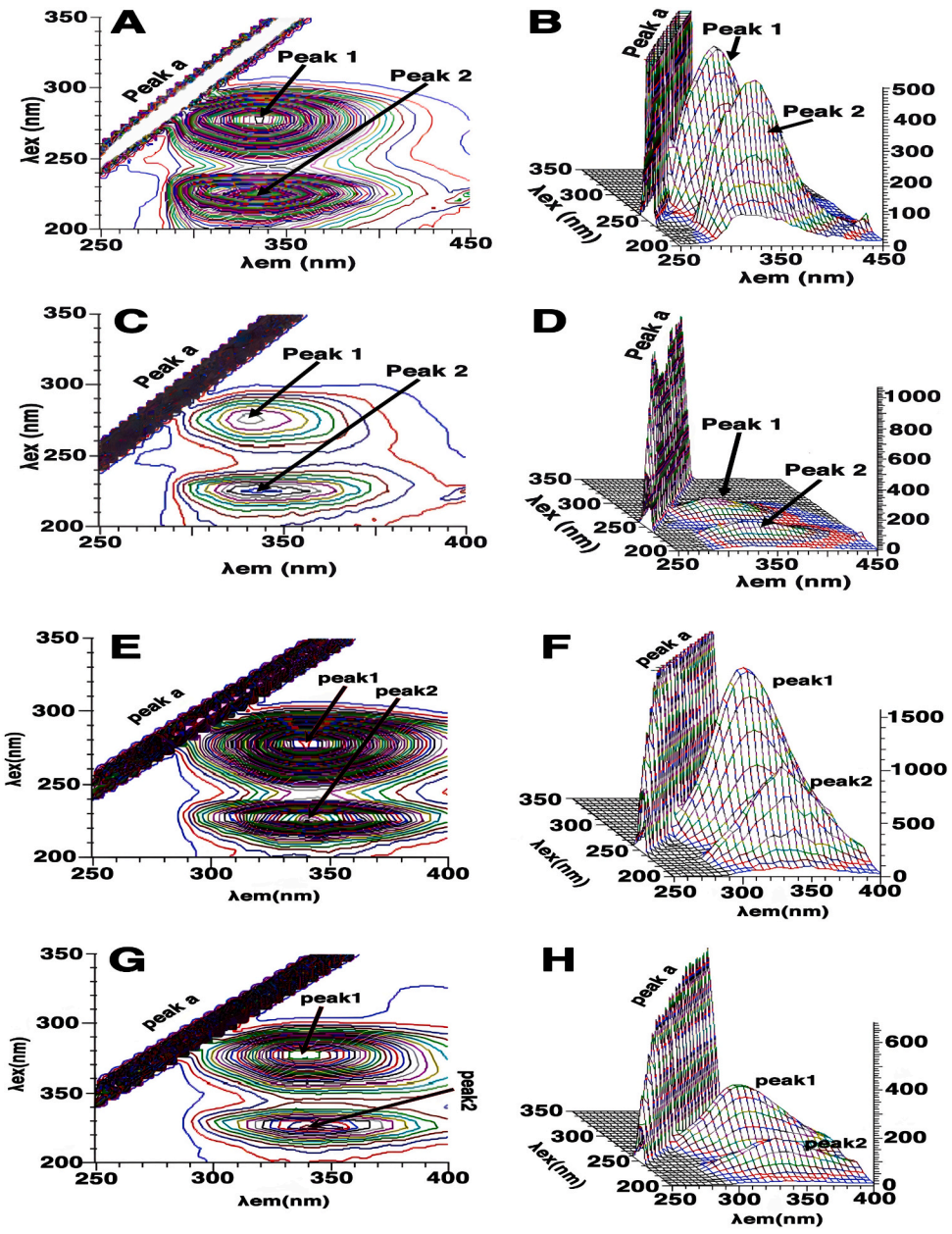

Fig. 11. Three dimensional fluorescence spectra of HSA (A: contour & B: birds eye mode), HSA-IndC (C: contour & D:birdseye mode) complex, BSA (E: contour & F: birdseye mode) and BSA-IndC (G: contour & H:birdseye mode) complex.

interactions for HSA while ALA A:290, LYS A:187, THR A: 190, TRP A:451, TYR A:156, TYR A:149, ARG A:256 and HIS A:241 are the residues in BSA that are involved in hydrophobic interactions (Fig. S6). Most of the amino acid residues present in the binding site exhibit a drastic change in accessible surface area [ΔASA(Å^2)] upon binding with IndC (Tables 4 & 5). The results indicate that the interacting residues are buried in hydrophobic pocket i.e. less available to solvent after interaction. Accessible surface area change [ΔASA(Å^2)] for HSA is 346.981Å^2 and for BSA is 344.475Å^2. Hydrogen bondings and hydrophobic interactions are the two main contributing forces which stabilize the HSA-IndC and BSA-IndC complex.

4.13. Discussion

The binding affinity of IndC with BSA was higher compared to HSA. For both cases complexation was predominantly enthalpy driven. Trp residues of HSA shifted to a more hydrophobic environment after complexation with IndC while the microenvironment of Trp and Tyr residues of BSA showed no significant change. In the context of IndC induced conformational change extent of decrease of α-helix was similar for both the serum albumins. More restriction was imposed upon Trp residue after complexation. The REES effect is more for HSA (10 nm) than BSA (4 nm) after complexation. This may be due to the fact that the structural rigidity of BSA is somewhat higher than HSA [68]. Theoretical study reveal that IndC preferably bind at site-I of both the serum proteins but free energy of binding is higher in case of BSA (−7.29 Kcal/mol) compared to HSA (− 6.41 kcal/mol) (table S2).

Dye and pigments are useful chemicals which are consumed by living beings directly or indirectly. Analysis of chemical interferences of these type of molecules in physiological systems is very important. Our present study aimed to establish a detailed understanding of the binding interaction between the serum proteins i.e. HSA & BSA and IndC. Several binding analyses involving this type of synthetic and natural food dye has been already reported. Phenazinium dye janus green blue,

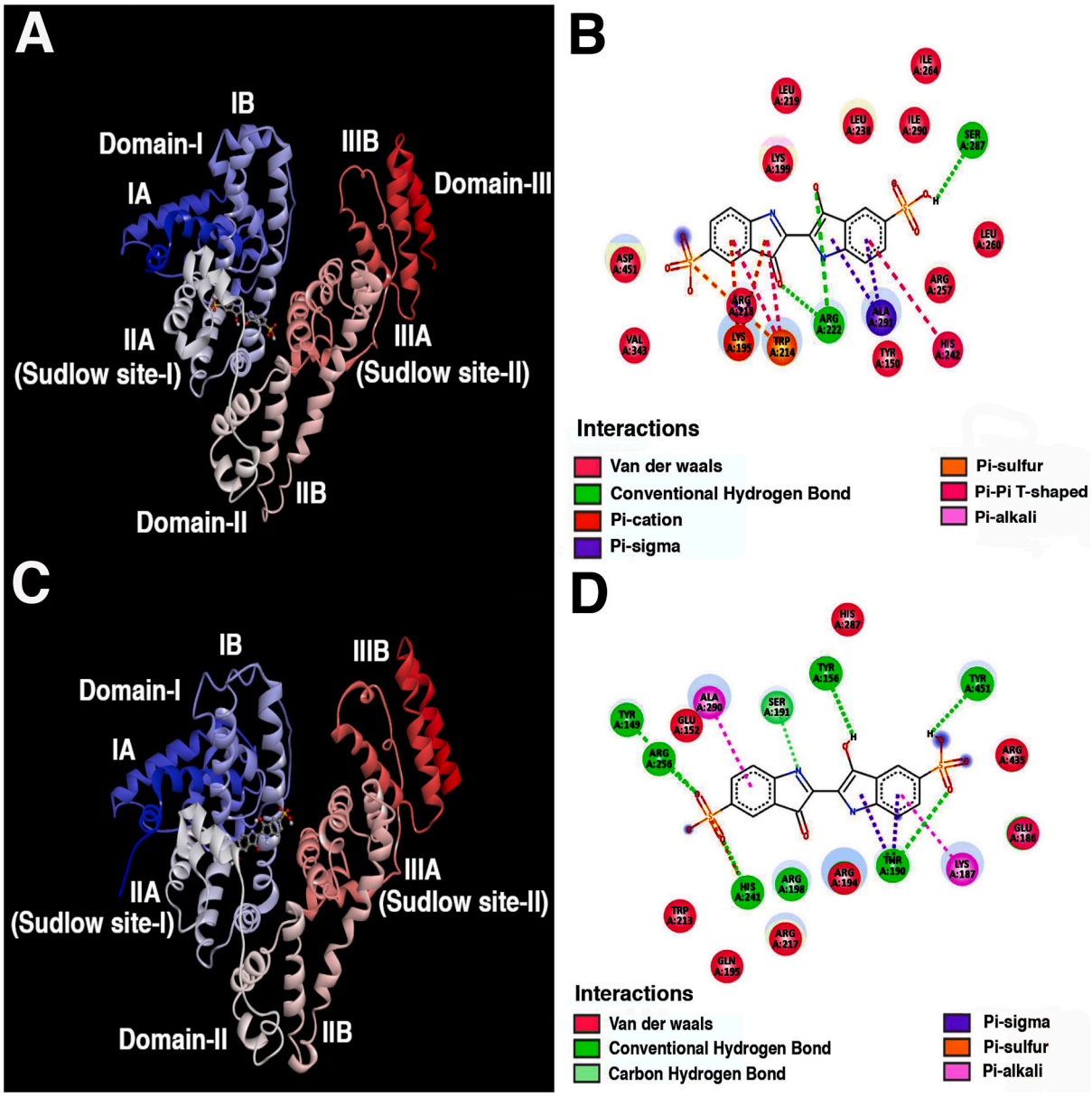

Fig. 12. Molecular docking of HSA-IndC (A & B) and BSA-IndC (C & D) complexes. A & C indicate the location of IndC in HSA & BSA, respectively, and B & D are the corresponding 2D images showing the interacting residues present in the binding site.

Table 4
Accessible surface area change of HSA per residue.

Residue	ASA of free HSA (Å^2)	ASA of HSA-IndC complex (Å^2)	ΔASA(Å^2)
TYR 150	18.407	6.22	12.187
LYS 195	88.247	49.392	38.855
LEU198	24.627	15.208	9.419
LYS 199	28.861	3.178	25.683
TRP 214	52.203	17.865	34.388
ARG 218	41.06	20.371	20.689
ARG 222	31.178	10.001	21.177
LEU 238	30.529	2.383	28.146
ARG 257	15.368	5.149	10.219
LEU 260	15.548	6.128	9.42
ILE 290	12.978	0.721	12.257
ALA 291	40.991	0.681	40.31
ASP 451	31.094	0.00	31.094
VAL 455	15.252	7.081	8.171

squaraine dye, azobenzene food dyes, amaranth, new coccine and tartrazine exhibit significant binding interaction with serum proteins [67,69–75]. Janus green blue (HSA: 13.80 × 10^4 M^{-1} & BSA: 28.40 × 10^4 M^{-1}), azo dyes tartrazine [HSA: (1.04 ± 0.05) × 10^5 M^{-1} & BSA: (1.92 ± 0.05) × 10^5 M^{-1})], amaranth [HSA: (1.76 ± 0.05) × 10^5 M^{-1} & BSA: (5.79 ± 0.07) × 10^5 M^{-1}] and phenothiazine dye toluidine blue O (HSA: 4 × 10^5 M^{-1} & BSA: 4.23 × 10^5 M^{-1}) shows comparable binding constant whereas IndC [HSA: (4.06 ± 0.30) × 10^4 & BSA: (9.39 ± 0.50) × 10^4 from ITC experiments] shows slightly lower binding constant value [67,69,74,75]. Therefore, IndC shows a moderate binding affinity towards serum protein. The complexation of tartrazine and amaranth with HSA & BSA was exothermic similar to IndC-HSA/BSA complexation whereas the complexation of janus green blue with HSA & BSA was endothermic. Literature survey revealed that static quenching mechanism was involved in tartazine-HSA/BSA, amaranth-HSA, toluidine blue O-HSA/BSA, janus green blue-HSA/BSA complexation whereas IndC exhibit a combined quenching mechanism (static & dynamic) with both HSA & BSA. In silico analysis revealed that amaranth, new coccine, toluidine blue O preferably bind at site-I (hydrophobic pocket of sub

Table 5
Accessible surface area change of BSA per residue.

Residue	ASA of free BSA (Å^2)	ASA of BAS-IndC complex (Å^2)	ΔASA(Å^2)
ASP 89	80.219	58.97	21.241
ILE 141	23.492	6.4659	17.023
ARG 144	46.519	36.873	9.646
TYR 149	13.969	0.34	13.929
GLU 152	11.29	0.0	11.29
GLU 186	75.874	63.942	11.932
LYS 187	114.565	75.039	39.526
LEU 189	73.079	59.8	13.279
THR 190	23.308	6.358	16.95
SER 191	18.282	0.077	18.282
ARG 194	75.421	33.146	42.275
ARG 198	26.996	6.15	20.846
ARG 217	67.284	40.114	27.17
LEU 237	24.741	9.987	14.754
HIS 287	22.973	11.898	11.075
ALA 290	52.897	6.469	46.428
GLU 291	122.22	110.986	11.236
ARG 435	65.581	50.535	15.046
TYR 451	41.776	17.735	24.041

domain-IIA) which is also comparable with IndC.

5. Conclusions

The results obtained indicate that fluorescence emission spectra of serum albumins were quenched through a combined quenching mechanism (i.e. static and dynamic). Though static quenching played the major role in the total quenching process but dynamic quenching can't be ignored as it appeared to be in the same order. High negative free energy value obtained from ITC experiments indicates spontaneous binding of IndC with serum proteins. FRET studies revealed that the protein-IndC binding distance (*r*) was 2.746 and 3.21 nms, respectively, for HSA and BSA. Synchronous fluorescence, 3D fluorescence, FTIR and CD revealed secondary structural changes and conformational alterations in HSA and BSA upon binding with IndC. Hydrophobic and hydrogen bonding interactions made major contributions towards the binding interaction. Molecular docking analysis revealed that sudlow site-I is the preferred binding site for IndC in both HSA and BSA. As mentioned earlier IndC is a diagnostic dye and food colorant and this study provides a deep insight into the molecular interaction between IndC and serum proteins which can help to understand its toxicological effects in biological and biomedical field for better healthcare applications.

CRediT authorship contribution statement

Gouranga Jana: Data curation, Investigation, Writing – original draft, Writing – review & editing, Formal analysis. **Shukdeb Sing:** Validation, Writing – original draft, Writing – review & editing. **Arindam Das:** Validation, Writing – original draft, Writing – review & editing. **Anirban Basu:** Conceptualization, Formal analysis, Funding acquisition, Supervision, Validation, Writing – original draft, Writing – review & editing.

Declaration of competing interest

The authors declare no competing financial interests exist.

Acknowledgements

AB & GJ acknowledge the financial support from the Department of Science and Technology and Biotechnology, Govt. of West Bengal (GO No.: 32(Sanc.)-ST/P/S&T/15G-13/2018 dated 31.01.2019). The authors thank DST, Govt. of India, for providing assistance and infrastructural support through the FIST program. The authors thank USIC, Vidyasagar University, for providing instrumental facilities. SS is a recipient of Junior Research Fellowship from UGC, Govt. of India.

Appendix A. Supplementary data

Supplementary data to this article can be found online at https://doi.org/10.1016/j.ijbiomac.2023.129143.

References

[1] Y. Ma, G. Zhang, J. Pan, Spectroscopic studies of DNA interactions with food colorant indigo carmine with the use of ethidium bromide as a fluorescence probe, J. Agric. Food Chem. 60 (2012) 10867–10875.
[2] J.D. Craik, D. Khan, R. Afifi, The safety of intravenous indigo carmine to assess ureteric patency during transvaginal uterosacral suspension of the vaginal vault, J. Pelvic Med. Surg. 15 (2009) 11–15.
[3] U.R. Lakshmi, V.C. Srivastava, I.D. Mall, D.H. Lataye, Rice husk ash as an effective adsorbent: evaluation of adsorptive characteristics for indigo carmine dye, J. Environ. Manage. 90 (2009) 710–720.
[4] M.C. Pagnacco, J.P. Maksimović, N.T. Nikolić, D.V. BajukBogdanović, M. M. Kragović, M.D. Stojmenović, S.N. Blagojević, J.V. Senćanski, Indigo carmine in a food dye: spectroscopic characterization and determining its micro-concentration through the clock reaction, Molecules 27 (2022) 4853.
[5] F.A. Hiawi, I.H. Ali, Study the adsorption behavior of food colorant dye indigo carmine and loratadine drug in aqueous solution, Chem. Methodol. 6 (2022) 720–730.
[6] A. Mittal, J. Mittal, L. Kurup, Batch and bulk removal of hazardous dye, indigo carmine from wastewater through adsorption, J. Hazard. Mater. 137 (2006) 591–602.
[7] I.C.de Sá, F.N. Feiteira, W.F. Pacheco, Quantification of the food dye indigo carmine in candies using digital image analysis in a polyurethane foam support, Food Anal. Methods 13 (2020) 962–969.
[8] R. Kammoolkon, N. Taneepanichskul, S. Taneepanichskul, Respiratory symptoms and their association with exposure to respiratory dust among indigo-dyed cotton workers, Arch. Environ. Occup. Health 77 (2022) 356–361.
[9] S. Kobylewski, M.F. Jacobson, Toxicology of food dyes, Int. J. Occup. Environ. Health 18 (2012) 220–246.
[10] E. Frumin, H. Velez, E. Bingham, M. Gillen, M. Brathwaite, R. LaBarck, Occupational bladder cancer in textile dyeing and printing workers: six cases and their significance for screening programs, J. Occup. Med. 32 (1990) 887–890.
[11] X.M. He, D.C. Carter, Atomic structure and chemistry of human serum albumin, Nature 358 (1992) 209–215.
[12] S. Curry, H. Mandelkow, P. Brick, N. Franks, Crystal structure of human serum albumin complexed with fatty acid reveals an asymmetric distribution of binding sites, Nat. Struct. Mol. Biol. 5 (1998) 827–835.
[13] A. Bujacz, Structures of bovine, equine and leporine serum albumin, Acta Crystallogr. D Biol. Crystallogr. 68 (2012) 1278–1289.
[14] S. Sugio, A. Kashima, S. Mochizuki, M. Noda, K. Kobayashi, Crystal structure of human serum albumin at 2.5 Å resolution, Protein Eng. 12 (1999) 439–446.
[15] S. Ketrat, D. Japrung, P. Pongprayoon, Exploring how structural and dynamic properties of bovine and canine serum albumins differ from human serum albumin, J. Mol. Graph. Model. 98 (2020) 107601.
[16] R. Maier, M.R. Fries, C. Buchholz, F. Zhang, F. Schreiber, Human versus bovine serum albumin: a subtle difference in hydrophobicity leads to large differences in bulk and interface behavior, Cryst. Growth Des. 21 (2021) 5451–5459.
[17] M.A. Bratty, Spectroscopic and molecular docking studies for characterizing binding mechanism and conformational changes of human serum albumin upon interaction with telmisartan, Saudi Pharm. J. 28 (2020) 729–736.
[18] L. Wang, X. Wu, Y. Yang, X. Liu, M. Zhu, S. Fan, Z. Wang, J. Xue, R. Hua, Y. Wang, Q.X. Li, Multi-spectroscopic measurements, molecular modeling and density functional theory calculations for interactions of 2,7-dibromocarbazole and 3,6-dibromocarbazole with serum albumin, Sci. Total Environ. 686 (2019) 1039–1048.
[19] Y. Wang, L. Wang, M. Zhu, J. Xue, R. Hua, Q.X. Li, Comparative studies on biophysical interactions between gambogic acid and serum albumin via multispectroscopic approaches and molecular docking, JOL 205 (2019) 210–218.
[20] Z. Zhao, T. Shi, Y. Chu, Y. Cao, S. Cheng, R. Na, Y. Wang, Comparison of the interactions of flupyrimin and nitenpyram with serum albumins via multiple analysis methods, Chemosphere 289 (2022) 133139.
[21] C. Bonechi, S. Martini, C. Rossi, Interaction study of indigo carmine with albumin and dextran by NMR relaxation, J. Mater. Sci. 46 (2011) 2541–2547.
[22] S. Tayyab, M.M. Izzudin, M.Z. Kabir, S.R. Feroz, W.V. Tee, S.B. Mohamad, Z. Alias, Binding of an anticancer drug, axitinib to human serum albumin: fluorescence quenching and molecular docking study, J. Photochem. Photobiol. B: Biol. 162 (2016) 386–394.
[23] A. Singha Roy, D.R. Tripathy, A. Chatterjee, S. Dasgupta, Spectroscopic study of the interaction of the antioxidant naringin with bovine serum albumin, J. Biophys. Chem. 1 (2010) 141–152.
[24] S.F. Sousa, P.A. Fernandes, M.J. Ramos, Protein-ligand docking: current status and future challenges, Proteins 65 (2006) 15–26.
[25] R. Huey, G.M. Morris, A.J. Olson, D.S. Goodsell, A semiempirical free energy force field with charge-based desolvation, J. Comput. Chem. 30 (2007) 1145–1152.
[26] P. Giannozzi, S. Baroni, N. Bonini, M. Calandra, R. Car, C. Cavazzoni, D. Ceresoli, G.L. Chiarotti, M. Cococcioni, I. Dabo, et al., QUANTUM ESPRESSO: a modular and

open-source software project for quantum simulations of materials, J. Phys. Condens. Matter 21 (2009) 395502.
[27] P. Hohenberg, W. Kohn, Inhomogeneous electron gas, Phys. Rev. 136 (1964) B864.
[28] J.P. Perdew, K. Burke, M. Ernzerhof, Generalized gradient approximation made simple, Phys. Rev. Lett. 77 (1996) 3865.
[29] J. Gasteiger, M. Marsili, A new model for calculating atomic charges in molecules, Tetrahedron Lett. 19 (1978) 3181–3184.
[30] G.M. Morris, D.S. Goodsell, R.S. Halliday, R. Huey, W.E. Hart, R.K. Belew, A. J. Olson, Automated docking using a lamarckian genetic algorithm and an empirical binding free energy function, J. Comput. Chem. 19 (1998) 1639–1662.
[31] A. Basu, G. Suresh Kumar, Binding and inhibitory effect of the dyes amaranth and tartrazine on amyloid fibrillation in lysozyme, J. Phys. Chem. B 121 (2017) 1222–1239.
[32] P. Chen, M. Shi, M. Niu, Y. Zhang, R. Wang, J. Xu, Y. Wang, Effects of HPPD inhibitor herbicides on soybean root exudates: a combination study of multispectral technique and 2D-COS analysis, Spectrochim. Acta Mol. Biomol. Spectrosc. 289 (2023) 122241.
[33] P. Chen, M. Shi, X. Liu, X. Wang, M. Fang, Z. Guo, X. Wu, Y. Wang, Comparison of the binding interactions of 4-hydroxyphenylpyruvate dioxygenase inhibitor herbicides with humic acid: insights from multispectroscopic techniques, DFT and 2D-COS-FTIR, Ecotox. Environ. Saf. 239 (2022) 113699.
[34] M. Marszalek, A. Konarska, E. Szajdzinska-Pietek, M. Wolszczak, Interaction of cationic protoberberine alkaloids with human serum albumin. No spectroscopic evidence on binding to Sudlow's site 1, J. Phys. Chem. B 117 (2013) 15987–15993.
[35] M.S. Ali, M. Amina, H.A. Al-Lohedan, N.M. Al Musayeib, Human serum albumin binding to the biologically active labdane diterpene "leoheterin": spectroscopic and in silico analysis, J. Photochem. Photobiol. B 182 (2018) 9–17.
[36] S. Bhuin, S. Halder, S.K. Saha, M. Chakravarty, Binding interactions and FRET between bovine serum albumin and various phenothiazine-anthracene−/based dyes: a structure–property relationship, RSC Adv. 11 (2021) 1679–1693.
[37] J.R. Lakowicz, G. Weber, Quenching of fluorescence by oxygen. A probe for structural fluctuations in macromolecules, Biochemistry 12 (1973) 4161–4170.
[38] H. Dezhampanah, M. Esmaili, S. Jampour, Spectroscopic and molecular docking studies on interaction of two schiff base complexes with bovine serum albumin, J. Biomol. Struct. Dyn. 38 (2020) 2650–2658.
[39] A.S. Tanwar, R. Parui, R. Garai, M.A. Chanu, P.K. Iyer, Dual "static and dynamic" fluorescence quenching mechanisms based detection of TNT via a cationic conjugated polymer, ACS Meas. Sci. Au 2 (2022) 23–30.
[40] M. Amiri, K. Jankeje, J.R. Albani, Characterization of human serum albumin forms with pH. Fluorescence lifetime studies, J. Pharm. Biomed. Anal. 51 (2010) 1097–1102.
[41] J.R. Lakowicz, Principles of Fluorescence Spectroscopy, 3rd ed, Plenum Press, 2006, pp. 277–285.
[42] M.D. Meti, K.S. Byadagi, S.T. Nandibewoor, S.D. Joshi, U.A. More, S. A. Chimatadar, In vitro studies on the interaction between human serum albumin and fosfomycin disodium salt, an antibiotic drug by multispectroscopic and molecular docking methods, Mol. Biol. Rep. 41 (2014) 2377–2387.
[43] M.B. Bolattin, S.T. Nandibewoor, S.D. Joshi, S.R. Dixit, S.A. Chimatadar, Interaction of hydralazine with human serum albumin and effect of β-cyclodextrin on binding: insights from spectroscopic and molecular docking techniques, Ind. Eng. Chem. Res. 55 (2016) 5454–5464.
[44] G.G. Ariga, P.N. Naik, S.A. Chimatadar, S.T. Nandibewoor, Interactions between epinastine and human serum albumin: investigation by fluorescence, UV–vis, FT–IR, CD, lifetime measurement and molecular docking, J. Mol. Struct. 1137 (2017) 485–494.
[45] S. Das, A. Rohman, A.S. Roy, Exploring the non-covalent binding behaviours of 7-hydroxyflavone and 3-hydroxyflavone with hen egg white lysozyme: multi-spectroscopic and molecular docking perspectives, J. Photochem. Photobiol. B Biol. 180 (2018) 25–38.
[46] S. Bi, L. Ding, Y. Tian, D. Song, X. Zhou, X. Liu, H. Zhang, Investigation of the interaction between flavonoids and human serum albumin, J. of Mol. Struct. 703 (2004) 37–45.
[47] P. Banerjee, S. Ghosh, A. Sarkar, S.C. Bhattacharya, Fluorescence resonance energy transfer: a promising tool for investigation of the interaction between 1-anthracene sulphonate and serum albumins, Luminescence 131 (2011) 316–321.
[48] S. Hadichegeni, B. Goliaei, M. Taghizadeh, S. Davoodmanesh, F. Taghavi, M. Hashemi, Characterization of the interaction between human serum albumin and diazinon via spectroscopic and molecular docking methods, Hum. Exp. Toxicol. 37 (2018) 959–971.
[49] R.N. El Gammal, H. Elmansi, A.A. El-Emam, F. Belal, M.E.A. Hammouda, Exploring the molecular interaction of mebendazole with bovine serum albumin using multi-spectroscopic approaches and molecular docking, Sci. Rep. 12 (2022) 11582.
[50] N. Shahabadi, S. Hadidi, Mechanistic and conformational studies on the interaction of a platinum(II) complex containing an antiepileptic drug, levetiracetam, with bovine serum albumin by optical spectroscopic techniques in aqueous solution, Appl. Biochem. Biotechnol. 175 (2015) 1843–1857.
[51] S. Hashempour, N. Shahabadi, A. Adewoye, B. Murphy, C. Rouse, B.A. Salvatore, C. Stratton, E. Mahdavian, Binding studies of aicar and human serum albumin by spectroscopic, theoretical, and computational methodologies, Molecules 25 (2020) 5410.
[52] D.M. Byler, H. Susi, Examination of the seconadary structure of proteins by deconvolved FTIR spectra, Biopolymers 25 (1986) 469–487.
[53] S. Krimm, J. Bandekar, Vibrational spectroscopy and conformation of peptides, polypeptides and proteins, J. Adv. Protein Chem. 38 (1986) 181–364.
[54] S. Dubeau, P. Bourassa, T.J. Thomas, H.A. Tajmir-Riahi, Biogenic and synthetic polyamines bind bovine serum albumin, Biomacromolecules 11 (2010) 1507–1515.
[55] Z. Cheng, R. Liu, X. Jiang, Spectroscopic studies on the interaction between tetrandrine and two serum albumins by chemometrics methods, Spectrochim. Acta A Mol. Biomol. Spectrosc. 115 (2013) 92–105.
[56] H.A. Alhazmi, FT-IR spectroscopy for the identification of binding sites and measurements of the binding interactions of important metal ions with bovine serum albumin, Sci. Pharm. 87 (2019) 5.
[57] G.D. Yang, C. Li, A.G. Zeng, Y. Zhao, R. Yang, X.L. Bian, Fluorescence spectroscopy of osthole binding to human serum albumin, J. Pharm. Anal. 3 (2013) 200–204.
[58] D. Wu, J. Wang, D. Liu, Y. Zhang, X. Hu, Computational and spectroscopic analysis of interaction between food colorant citrus red 2 and human serum albumin, Sci. Rep. 9 (2019) 1615.
[59] A. Basu, G.S. Kumar, Study on the interaction of the toxic food additive carmoisine with serum albumins: a microcalorimetric investigation, J. Hazard. Mater. 273 (2014) 200–206.
[60] P.D. Ross, S. Subramanian, Thermodynamics of protein association reactions: forces contributing to stability, Biochemistry 20 (1981) 3096–3102.
[61] A. Basu, G.S. Kumar, Interaction and inhibitory influence of the azo dye carmoisine on lysozyme amyloid fibrillogenesis, Mol. Biosyst. 13 (2017) 1552–1564.
[62] N.J. Greenfield, Using circular dichroism spectra to estimate protein secondary structure, Nat. Protoc. 1 (2006) 2876–2890.
[63] A.J. Miles, B.A. Wallace, Circular dichroism spectroscopy of membrane proteins, Chem. Soc. Rev. 45 (2016) 4859–4872.
[64] M. Qureshi, S. Javed, Investigating binding dynamics of trans resveratrol to HSA for an efficient displacement of aflatoxin B_1 using spectroscopy and molecular simulation, Sci. Rep. 12 (2022) 2400.
[65] A. Chattopadhyay, S. Haldar, Dynamic insight into protein structure utilizing red edge excitation shift, Acc. Chem. Res. 47 (2014) 12–19.
[66] L. Shang, Y. Wang, J. Jiang, S. Dong, pH-dependent protein conformational changes in albumin:gold nanoparticle bioconjugates: a spectroscopic study, Langmuir 23 (2007) 2714–2721.
[67] A.S. Selva Sharma, S. Anandakumar, M. Ilanchelian, A combined spectroscopic and molecular docking study on site selective binding interaction of toluidine blue o with human and bovine serum albumins, JOL 151 (2014) 206–218.
[68] V. Mishra, R.J. Heath, Structural and biochemical features of human serum albumin essential for eukaryotic cell culture, Int. J. Mol. Sci. 22 (2021) 8411.
[69] S. Saha, S. Bhattacharjee, J. Chowdhury, Exploring the binding interactions of janus green blue with serum albumins from spectroscopic and calorimetric studies aided by in silico calculations, J. Biomol. Struct. Dyn. 40 (2022) 5328–5344.
[70] V.S. Jisha, K.T. Arun, M. Hariharan, D. Ramaiah, Site-selective interactions: squaraine dye-serum albumin complexes with enhanced fluorescence and triplet yields, J. Phys. Chem. B 114 (2010) 5912–5919.
[71] O.A. Chaves, R.J.S. Loureiro, A. Costa-Tuna, Z.L. Almeida, J. Pina, R.M.M. Brito, C. Serpa, Interaction of two commercial azobenzene food dyes, amaranth and new coccine, with human serum albumin: biophysical characterization, ACS Food Sci. Technol. 3 (2023) 955–968.
[72] X. Pan, P. Qin, R. Liu, J. Wang, Characterizing the interaction between tartrazine and two serum albumins by a hybrid spectroscopic approach, J. Agric. Food Chem. 59 (2011) 6650–6656.
[73] G. Zhang, Y. Ma, Mechanistic and conformational studies on the interaction of food dye amaranth with human serum albumin by multispectroscopic methods, Food Chem. 136 (2013) 442–449.
[74] A. Basu, G.S. Kumar, Targeting proteins with toxic azo dyes: a microcalorimetric characterization of the interaction of the food colorant amaranth with serum proteins, J. Agric. Food Chem. 62 (2014) 7955–7962.
[75] A. Basu, G.S. Kumar, Thermodynamics of the interaction of the food additive tartrazine with serum albumins: a microcalorimetric investigation, Food Chem. 62 (2015) 137–142.